JOURNAL OF CATALYSIS **173,** 247–256 (1998)
ARTICLE NO. CA971942

Ni/Mg/Al Anionic Clay Derived Catalysts for the Catalytic Partial Oxidation of Methane

Residence Time Dependence of the Reactivity Features

F. Basile,* L. Basini,*,†,[1] M. D' Amore,* G. Fornasari,* A. Guarinoni,† D. Matteuzzi,* G. Del Piero,‡ F. Trifirò,* and A. Vaccari*

*University of Bologna, Department of Industrial Chemistry and Materials, Viale Risorgimento 4, 40136 Bologna, Italy; †Snamprogetti Research Laboratories, Via Maritano 26, 20097, San Donato Milanese (MI), Italy; and ‡Eniricerche Research Laboratories, Via Maritano 26, 20097, San Donato Milanese (MI), Italy

Received November 14, 1996; revised August 4, 1997; accepted October 22, 1997

The catalytic partial oxidation (CPO) of methane was investigated with four Ni-based catalysts prepared through reduction of hydrotalcite-type precursors. The calcination of the precursors, generated materials in which the Ni species were differently distributed between NiO, (Ni, Mg)Al_2O_4 phases and NiO–MgO periclase structures. The relative amount of the different phases depended on Ni content and affected the reactivity of the solids towards reduction and towards CPO step. Catalysts with high Ni-content required mild reduction conditions, but deactivated rapidly with time-on-stream due to carbon formation. Instead, catalysts with low Ni-content were activated only after a severe reduction treatment but showed high stability during the reaction. The effect of residence time was investigated with a particularly stabilized catalyst, in order to understand if selectivities and conversions could be kinetically controlled. Results were grouped considering three reactivity regions ($\tau \leq 70$ ms, $70 < \tau < 150$ ms, and $300 < \tau < 720$ ms). In the shorter residence time region, large chemical composition variations and large temperature gradients were observed along the catalytic bed and relevant differences between surface and gas temperatures were determined. These differences, not observed in the other two residence time regions, are discussed and related to heat transfer limitation, occurrence of direct oxidation routes and hot spot phenomenon effects.

Key Words: **methane; catalytic partial oxidation; syngas; nickel catalysts; anionic clays.**

1. INTRODUCTION

The catalytic partial oxidation of methane (CPO) [1] is a mild exothermic reaction which has been recently (1–6). re-investigated after the discovery that the catalytic process can occur at very short residence time ($\tau \cong 10^{-3}$ s) on the surface of different transition metal containing catalysts. Some of the points to be investigated and understood concern the reasons why methane conversions and CO and H_2 selectivity are so high and why the turnover frequency values overcome of one order of magnitude or more the values of the known heterogeneous and homogeneous phase catalytic processes,

$$CH_4 + \tfrac{1}{2}\,O_2 \rightarrow CO + 2\,H_2 \quad (\Delta H^\circ 298 = -35.5\,\text{kJ/mol}). \quad [1]$$

As pointed out by Lunsford *et al.* (7), CPO was studied since 1946, when it was first published that Ni-containing catalysts where able to produce syngas from methane and oxygen mixtures (8). For many years, the reaction pathway was described with a mechanism involving two steps: (a) the total catalytic combustion of methane in the oxygen-rich zone of the reactor yielding carbon dioxide and water [2], (b) the reforming of the remaining methane with steam [3] or carbon dioxide [4]:

$$CH_4 + 2\,O_2 \rightarrow CO_2 + 2\,H_2O \quad (\Delta H^\circ 298 = -801.7\,\text{kJ/mol}) \quad [2]$$

$$CH_4 + CO_2 \rightarrow 2\,CO + 2\,H_2 \quad (\Delta H^\circ 298 = +247.5\,\text{kJ/mol}) \quad [3]$$

$$CH_4 + H_2O \rightarrow CO + 3\,H_2 \quad (\Delta H^\circ 298 = +206\,\text{kJ/mol}). \quad [4]$$

These assumptions have been recently revisited by many authors (1–7, 9–11) who investigated the relations between: (a) surface activation energies and selectivities (1–3); (b) surface temperature and gas temperature values (10–11); (c) surface composition and product selectivity values (9).

In this study the attention is focused on: (a) the stabilization of small nickel clusters, which are not deactivated by the carbon formation reactions at 1 atm; (b) the temperature

[1] E-mail: LUCA.BASINI@SNAMPRO.ATLAS.IT.

0021-9517/98 $25.00

gradients and chemical composition variation along the catalytic bed; (c) the differences between reactivity features measured in a wide range of residence time values between 720 and 3.6 ms.

Main results concern: (a) the definition of catalyst preparation procedures which allow stabilization of Ni based catalysts during CPO at 1 atm, (b) experimental findings on the occurrence of discontinuity in the chemical and physical phenomena which originate CPO at the different residence time values.

2. EXPERIMENTAL

Catalysts Preparation

Four $Ni_x\ Mg_{(71-x)}\ Al_{29}$ catalysts, where $x = 10$, 34, 61, 71 (atomic ratio percentage, hereafter referred to as Ni_{10}, Ni_{34}, Ni_{61}, and Ni_{71}) where prepared by coprecipitation at $pH = 8.0$, pouring under energetic stirring a solution of the nitrates of the elements into a solution containing a slight excess of $NaHCO_3$. The precipitates were stirred at 333 K for 30 min, then filtered and washed with water until the sodium content was lower than 0.02% (w/w, as Na_2O). The precipitates were dried at 363 K overnight and then calcined at 1173 K for 16 h; the powdered materials were pressed into pellets which were then crushed to produce particles with dimensions between 600–850 μm.

Catalyst Characterization

These samples have been extensively characterized in previous works (12, 13). Here some of the XRD, TPR, and surface area measurements have been repeated to ensure the reproducibility of the preparation methods. The XRD patterns were taken with a Philips PW 1050/81 diffractometer controlled by a PW 1710 unit, using a Ni-filtered CuKα radiation ($\lambda = 0.15418$ nm) (40 kV, 40 mA). A 2θ range from 10 to 80° was investigated at a scanning speed of 60°/h. The lattice parameters were determined by least-squares refinements, from the well-defined position of the five most intense peaks. The crystallite sizes of the hydrotalcite-type (HT), oxide, and spinel phases were determined by the Scherrer equation using the average values of [(003) and (006)], [(200) and (220)], and [(220) and (400)] line widths. The Warren correction was used for instrumental line broadening, while the possible contribution of disorder effects and/or lattice strains was not taken into account. Quantitative phase analysis and structure determination was performed, in one experiment, on samples taken from different sections of the catalytic bed. The analysis was developed according to the Rietveld profile fitting method (14) applying the procedure proposed by Hill and Howard (15). Calculations were performed using the WRYET package (16). Structural data were taken from Wyckoff (17).

Chemical composition was also monitored with SEM-EDS (scanning electron microscopy—energy dispersive spectroscopy) using a Jeol 5400LV microscope equipped with EDAX PV 9900 analyzer.

Surface areas were determined by N_2 adsorption measurements performed with a Carlo Erba Sorpty model 1750 apparatus. Temperature programmed reduction (TPR) profiles of the samples (10 to 15 mg) calcined at 1173 K were obtained with a Perkin Elmer TGS-2 thermobalance according to procedures described in Ref. (18). All runs were conducted in a flowing H_2/He mixture (33 : 67 v/v) at atmospheric pressure, using a flow rate of 3.0 dm^3/h. Temperature was varied between 623–1173 K using a heating rate of 600 K/h; the weight losses due to the reaction [5] were recorded as a function of the temperature. Preliminary tests of water adsorption and desorption on calcined materials showed that water was not adsorbed (or fully desorbed) at temperatures higher than 473 K,

$$NiO + H_2 \rightarrow Ni^0 + H_2O. \qquad [5]$$

Reactivity Tests and Temperature Measurements

Catalytic tests were performed with two quartz fixed-bed reactors; one with a 4 mm ID, and the other 15 mm ID. The quartz reactors were immersed in two 500 W electrically heated furnaces and were operated at atmospheric pressure. In a first operation mode (used with the smaller reactor equipment) the oven temperature was kept constant while the reaction temperature was allowed to vary according to the exothermicity of the reactions. In a second operation mode (used with the larger reactor), the maximum reaction temperature was kept at a constant value by varying the heating power.

In the smaller reactor, temperature was measured with one 0.5-mm chromel-alumel thermocouple inserted into a quartz thermocouple well at the center of the catalytic bed. In the larger reactor gas temperature was measured with two movable 0.5-mm chromel-alumel thermocouples inserted into a quartz thermocouple well while surface temperatures were measured with an IR thermography equipment (AGEMA) which collected and analyzed the IR emitted radiation in the 2–5 μm range.

Weighted amounts of catalyst particles (between 25 and 200 mg in the 4-mm ID reactor and 1500 mg in the 15-mm ID reactor) were placed in the middle of reactor tubes, between two layers of corundum particles. Residence time was modified by adjusting either the flow rate of the feedstock or the amount of catalyst. Catalysts were activated *in situ* at 773 or at 1023 K for 4–8 h in a flowing H_2/N_2 mixture (50/50 v/v). Reaction products were analyzed on line, after condensation of water at 273 K, using two gaschromatographs equipped with HWD and Carbosieve S-II 100–120 mesh-packed columns; N_2 and He were used as carrier gases respectively in the analysis of H_2 and of the other

TABLE 1

Atomic ratios	Identified crystallographic phases	Crystal size (nm)	Lattice parameter a (nm)	Lattice parameter c (nm)	Surface area after drying at 363 K (m^2/g)
Ni/Mg/Al = 10/61/29	Hydrotalcite	9.0	0.3042(7)	2.285(7)	97
Ni/Mg/Al = 34/37/29	Hydrotalcite	7.5	03039(7)	2.295(9)	73
Ni/Mg/Al = 61/10/29	Hydrotalcite	7.0	0.3037(4)	2.291(4)	74
Ni/Mg/Al = 71/0/29	Hydrotalcite	4.5	0.3035(7)	2.293(7)	100

products (CO, CO_2, O_2, and CH_4). The thermodynamic data at equilibrium were calculated via a sensitivity analysis using the Aspen Technology software Aspen Release 9.2. The CH_4 and O_2 conversion values (X_{CH_4} and X_{O_2}, respectively) and CO and H_2 selectivities (S_{CO} and S_{H_2}, respectively) were calculated according to the formulas,

$$X_{CH_4} = \frac{F_{CH_{4in}} - F_{CH_{4out}}}{F_{CH_{4in}}} * 100$$

$$= \frac{F_{CO_{out}} + F_{CO_{2out}}}{F_{CO_{out}} + F_{CO_{2out}} + F_{CH_{4out}}} * 100$$

$$X_{O_2} = \frac{F_{O_{2in}} - F_{O_{2out}}}{F_{O_{2in}}}$$

$$= \frac{0.5 * F_{CO_{out}} + 0.5 * F_{H_2O_{out}} + F_{CO_{2out}}}{0.5 * F_{CO_{out}} + 0.5 * F_{H_2O_{out}} + F_{CO_{2out}} + F_{O_{2out}}} * 100$$

$$S_{CO} = \frac{F_{CO_{out}}}{F_{CO_{out}} + F_{CO_{2out}}} * 100$$

$$S_{H_2} = 0.5\frac{F_{H_{2out}}}{F_{CO_{out}} + F_{CO_{2out}}} * 100.$$

3. RESULTS

Physicochemical Characterization

The compositions, the identified phases, their crystallographic parameters, and the surface areas values of the samples dried at 363 K or calcined at 1173 K are reported in Tables 1 and 2, respectively. As previously reported (12, 13), the XRD patterns of the four coprecipitated precursors showed only the presence of a well-crystallized HT phase (Table 1), with parameters which are well correlated with the M^{2+}/M^{3+} ratio and the nature of ions present (18, 19). The XRD patterns and the lattice parameters measured after calcination at 1173 K, showed for the Ni-rich samples (Ni_{61} and Ni_{71}) the segregation of NiO and a spinel (Ni, Mg)Al_2O_4 or $NiAl_2O_4$ phase, while for the samples with lower Ni-contents (Ni_{10} and Ni_{34}) the formation of NiO–MgO solid solutions (20, 21) and a spinel $MgAl_2O_4$ phase were observed (Table 2).

According to the XRD data, the TPR analyses performed on the samples calcined at 1173 K showed for the Ni-rich catalysts (Ni_{61} and Ni_{71}) a first broad reduction peak with maxima respectively at 820 and 800 K, typical of the reduction of NiO (22, 23) and a second peak, which was still growing at $T > 1300$ K (the instrumental limit of the heater). This last peak can be assigned, according to previous works (13, 24), to the reduction of the $NiAl_2O_4$ phase. On the other hand, the Mg-rich catalysts (Ni_{10} and Ni_{34}) showed different reactivity features, exhibiting only a high temperature reduction peak (observed respectively at 1160 for Ni_{10} and 1190 K for Ni_{34}), due to the reduction of Ni-containing species inside an inert matrix (12, 13, 25, 26).

Catalytic Partial Oxidation Tests: Activation and Deactivation

The HT precursors calcined at 1173 K were submitted to a mild reductive pretreatment in which the catalysts were heated at 773 K for 4 h in a flowing H_2/N_2 (50 : 50 v/v) stream. Subsequently, at the same oven temperature, a CH_4/O_2/He mixture (2/1/4 v/v) was flowed through the reduced catalyst maintaining a residence time (τ) equal to 45 ms. Following this mild reductive pretreatment the Ni_{71} and Ni_{61} samples were found to be much more reactive towards CPO (S_{CO} and S_{H_2} above 80%) than the Ni_{34} and the Ni_{10} samples (S_{CO} and S_{H_2} below 35%); however, the Ni-rich catalysts were completely deactivated after 2–3 h of time-on-stream. By increasing the temperature of the reductive pre-treatment at 1023 K, the reactivity of the Ni_{34} catalyst was strongly improved and became analogous to those of the Ni-rich samples before deactivation; while the reactivity of the Ni_{10} catalyst showed the same improvement only after an 8 h reduction treatment at 1023 K.

TABLE 2

Atomic ratios	Identified crystallographic phases	Oxide crystal size (nm)	Spinel crystal size (nm)	Oxide lattice parameter a (nm)	Spinel lattice parameter a (nm)	Surface area after calcination at 1173 K (m^2/g)
Ni/Mg/Al = 10/61/29	(Ni, Mg)O + $MgAl_2O_4$	14.5	18.5	0.4205(2)	0.8080(5)	53
Ni/Mg/Al = 34/37/29	(Ni, Mg)O + $MgAl_2O_4$	15.5	16.0	0.4195(3)	0.8056(5)	47
Ni/Mg/Al = 61/10/29	NiO + (Ni, Mg)Al_2O_4	12.0	19.0	0.4178(4)	0.8048(3)	39
Ni/Mg/Al = 71/0/29	NiO + $NiAl_2O_4$	14.5	16.0	0.4177(2)	0.8051(3)	27

However, unlike the Ni-rich samples, these last two catalysts did not show any deactivation phenomena during an 8-h test.

Due to its stability under reaction conditions the Ni_{10} catalyst was selected to investigate the changes in the reactivity as a function of the residence time (between 3.6 and 760 ms), feed composition [$CH_4/O_2/He = 2/1/4$ or 2/1/20 (v/v)] and heater temperature.

Short Residence Time Reactivity Features in the Reactor with 4 mm ID

Tests at residence times between 3.6 and 72 ms were performed maintaining at two constant values the oven temperatures (1023 and 773 K) and allowing the reaction temperature to vary according to the exothermicity of the reactions. In a first experimental sequence at oven temperature of 1023 K, the reactor was fed with a $CH_4/O_2/He =$ 2/1/4 (v/v) mixture. At this oven temperature CPO reaction immediately ignited and reaction temperatures at the center of the catalytic bed when stationary conditions were attained were always above 1023 K (see Fig. 1A). The highest temperature value was measured at the shortest residence time value (1165 K at $\tau = 3.6$ s). Oxygen conversion was always complete, while methane conversion and CO and H_2 selectivity were higher than 90%. Product exit stream composition closely approached the equilibrium values.

The same reactivity tests were repeated maintaining the oven temperature at 773 K. Also in this case reactions were easily ignited and the measured temperatures, in stationary conditions, were between 800 and 1000 K (the maximum value, 1030 K was measured at $\tau = 3.6$ s; see Fig. 1B). However, selectivities and conversions were clearly shifted from the ones predicted by thermodynamics. In particular, methane conversion and selectivities in CO and H_2 decreased, whereas those in CO_2 and H_2O increased.

The tests at the two oven temperatures were also repeated by feeding the reactor with a more diluted reaction mixture ($CH_4/O_2/He = 2/1/20$ v/v). With an oven temperature of 1023 K, methane conversion and selectivities (exceeding the 90%) were not so different from the ones obtained with the less diluted feedstock and were close to those predicted by equilibrium calculations (Fig. 1C). However, by reducing the oven temperature at 773 K and repeating again the reactivity tests, the product composition shifted from the equilibrium more markedly than in the case of the lower He-content feed (Fig. 1D). The maximum reaction temperature was measured at $\tau = 3.6$ ms.

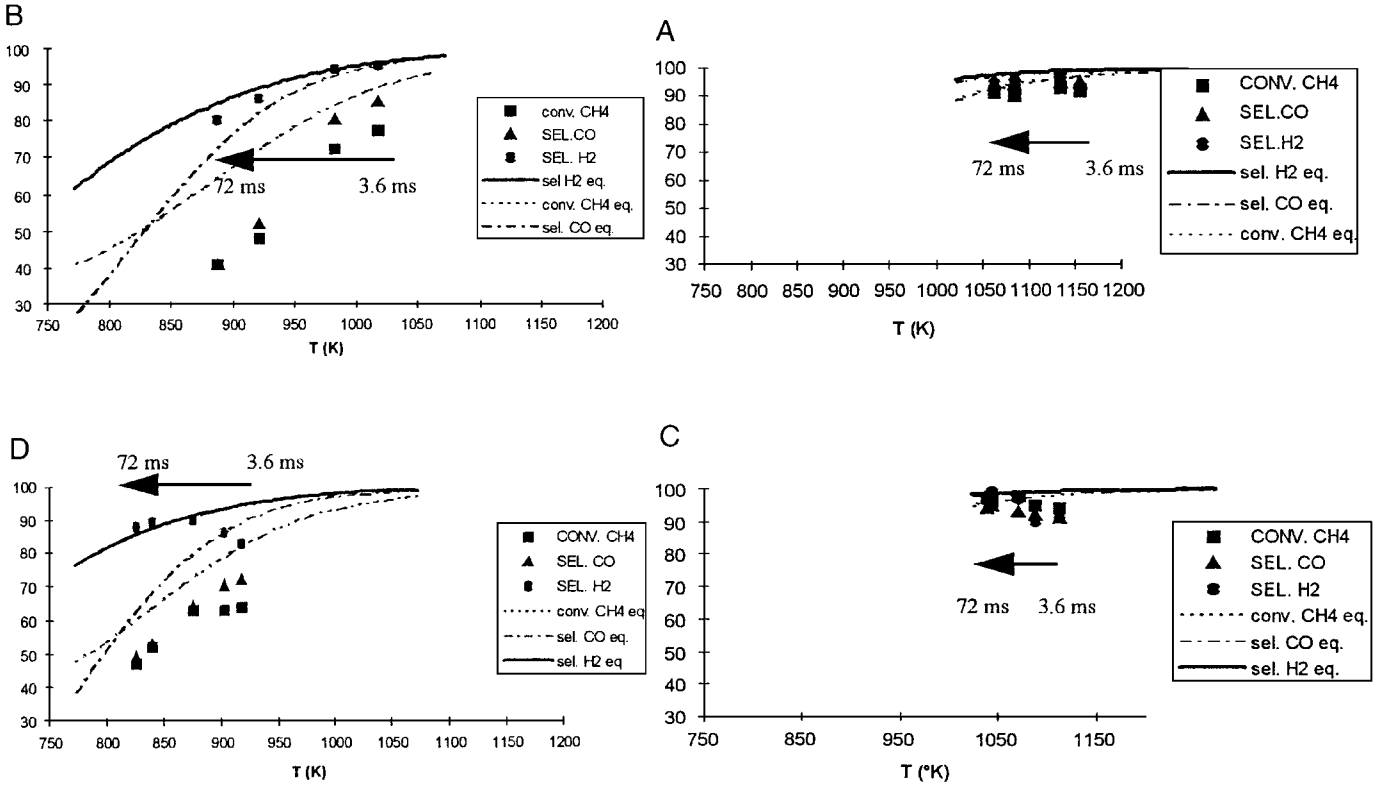

FIG. 1. Experimental and thermodynamic values of conversion and selectivities as a function of the residence time, oven temperature, and feed composition: (A) reaction mixture $CH_4/O_2/He = 2/1/4$ (v/v), oven temperature = 1023 K; (B) reaction mixture $CH_4/O_2/He = 2/1/4$ (v/v), oven temperature = 773 K; (C) reaction mixture $CH_4/O_2/He = 2/1/20$ (v/v), oven temperature = 1023 K; (D) reaction mixture $CH_4/O_2/He = 2/1/20$ (v/v), oven temperature = 773 K.

It is pointed out that during the tests performed in the 4 mm ID reactor, the rate of heat dispersion through the reactor walls (≅0.5 W in the catalytic zone) was estimated to be comprised between 36 and 22% of the rate of heat production (between 1.4 and 2.3 W) and reaction temperatures could be significantly affected by the amount of external heat supply. These facts allowed to appreciate the influence of temperature on reactivity features and particularly on the approach to equilibrium conditions.

Reactivity Features Observed with a 15 mm ID Reactor at Residence Time between 720 and 13 ms

Another set of experiments was performed with τ variations between 13 and 720 ms in a larger quartz reactor (ID 15 mm, catalyst amount 1.5 g). The reactor was fed with a $CH_4/O_2/He = 2/1/4$ v/v gas mixture and the maximum reaction temperature was maintained close to 973 K by varying (or, in one limit, switching off) the external heating. Moreover, at residence time $\tau = 13$ ms, the heating furnace was lifted above the catalytic zone in order to allow surface temperatures measurements with IR thermography.

Reactivity features will be reported considering three residence time ranges: At $720 \geq \tau \geq 300$ ms, in stationary conditions, both reactant conversions and product selectivities were fairly close to equilibrium values estimated at 973 K. Longitudinal temperature gradients along the catalytic bed were small. In particular at 360 ms the meximum temperature value (982 K) was detected in the first half of the catalytic bed; while the lower temperature value (965 K) was measured at the end of the catalytic bed. At 360 ms reactivity features were as follows: % CH_4 conv. = 84; % H_2 sel. = 92; % CO sel. = 89. Reactions could not be self-sustained without an external heat supply; in fact the rate of reaction heat production was comprised between 4 and 10 W, which was an amount comparable with the heat dispersion rate from the reaction zone (≅4 W).

Reduction of residence time from 300 to 72 ms also reduced conversion and selectivities, even if temperature values measured along the thermocouple well were maintained close to 973 K by adjusting the external heat supply. In these τ conditions longitudinal temperature variations along the bed were limited to 20 K. In particular, we mention that at 72 ms we measured % CH_4 conv. = 72; % H_2 sel. = 89.9%; % CO sel. = 83.3%.

Conversions and selectivities raised again close to values predicted by thermodynamic equilibria at 973 K by further reducing the residence time to values below 70 ms. Below 25 ms CH_4 conversion values were comprised between 85 and 90% and selectivities towards syngas were above 90%. The heater was switched off at τ below 25 ms in order to prevent reaction temperatures from raising above 973 K and the reactions remained self-sustained. Differently from what occurred in the other tests at higher residence time, very large longitudinal temperature variations (≅200 K) were determined along the catalytic bed and the highest temperature (975 K) was reached at the end of the catalytic bed. Precise temperature measurements along the catalytic bed became critical and for this reason thermocouples and IR thermography were simultaneously used to estimate reactions temperatures. The results of these measurements will be described for a test performed at $\tau = 14$ ms. In this case the collection of IR emitted radiation was obtained by lifting the cool heater assembly above the catalytic zone. The removal of the heater shielding increased the rate of heat transfer through the reactor walls (heat dispersion rate was estimated to increase from 14 to 17 W) and caused an overall reduction of the reaction temperature. However, the rate of heat production (170 W) was still sufficient to sustain CPO. Thermocouples detected a temperature decrease from 973 to 934 K and from 770 to 687 K at the end and at the entrance of the catalytic bed, respectively. Table 3 reports the main indications on reactivity features obtained after the removal of the heater from the catalytic zone. The temperature decrease was not only accompanied by a reduction in CH_4 conversion and selectivity toward syngas but also by oxygen leakage into the output stream. These findings indicate that the observed reactions were largely confined at the surfaces.

TABLE 3

	% mole in	% mole out	
CH_4	30.0	9.9	% conv. $CH_4 = 59.7$
O_2	15.0	1.1	% conv. $O_2 = 91.1$
N_2	55.0	45.3	% sel CO = 78.0
CO	0	11.4	% sel $H_2 = 82$
CO_2	0	2.7	$H_2/CO = 2.1$ v/v
H_2	0	24.1	v gas in = 1.09 m/s
H_2O	0	5.5	v gas out = 1.44 m/s
			$\tau = 14$ ms
			catalyst amount = 1.6 g

A visual inspection of the reaction zone allowed to see that the last part of the catalytic bed was incandescent. Figures 2 and 3 show the surface temperature mapping profiles obtained with IR thermography. Surface temperatures resulted higher than gaseous temperatures. Differences were particularly remarkable, at the end of the incandescent catalytic bed where the maximum surface temperature value was 1020 K and maximum gas temperature was 934 K. At the entrance of the catalytic bed surface temperatures had an average value of 740 K while the gas temperature was 687 K.

The surface temperature measurements required to estimate: (a) the percentage of IR emission transmitted through the quartz wall in the 2–5 μm range (85%); (b) the emissivity (ε) of the catalytic surfaces. Emissivity varied along the catalytic bed due to changes in the catalyst composition as determined with a chemical and phase composition analysis of the spent catalyst.

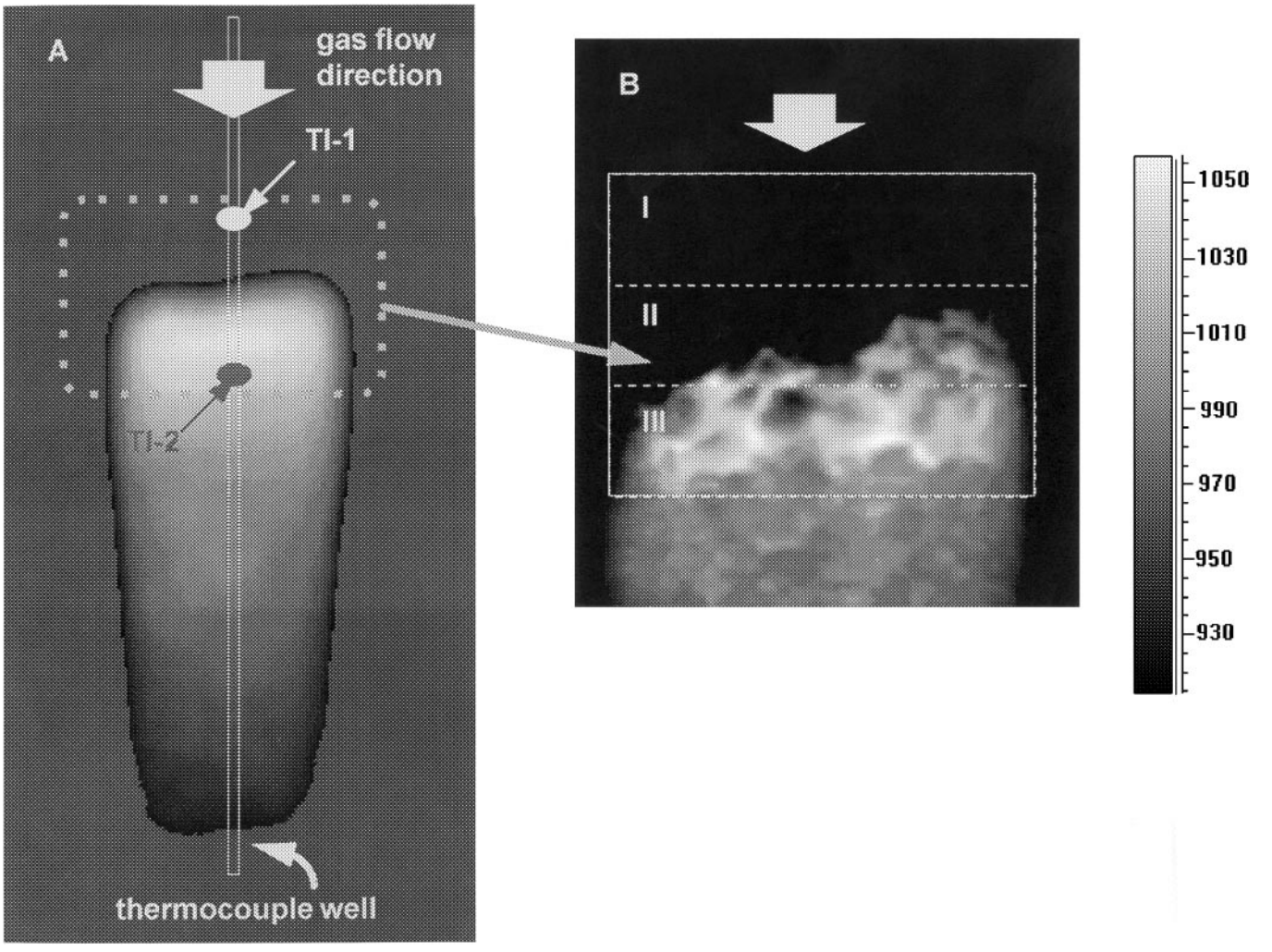

FIG. 2. IR thermography images of the reactor (A) and of the catalytic bed (B) during a 14-ms residence time test. TI-1 and TI-2 indicate the position of two thermocouples which contemporaneously measured gas temperatures. Zones I, II, III of the catalytic bed were analyzed for chemical and phase composition according to the text description.

The spent catalytic bed was in fact divided into three fractions (see Fig. 2B) which also showed a different color; the three fractions are named head (greenish), middle (dark greenish), and tail (dark gray). SEM-EDS and XRD analysis showed that the three fractions had the same content of Ni, Al, Mg (Ni/Mg/Al = 10/61/29 atomic ratios) and that the amount of these metals was not varied with respect to the HT precursor. On the contrary XRD quantitative phase composition analysis and structural refinement by Rietveld method detected four phases whose relative amounts varied along the catalytic bed (see Tables 4, 5 and Fig. 4). The four phases were: (a) Ni metal, (b) NiO–MgO peryclase, (c) $MgAl_2O_3$ spinel, and (d) graphitic carbon.

Despite SEM-EDS analysis showed that the amount of Ni/Mg/Al remained the same, XRD analysis indicated that the quantity of total Ni (Ni + NiO phases) increased from head to tail of the catalytic bed. Conversely, MgO decreased and $MgAl_2O_4$ remained at a constant value which was 6 wt% lower than the amount expected from chemical analysis data. For instance, in the case of the tail side of the catalytic bed, quantitative phase analysis gave Ni : MgO : $MgAl_2O_3$ = 11 : 49 : 40, instead of the

TABLE 4

	Ni (metal)	NiO	MgO	$MgAl_2O_4$
Head	3.2	3.2	54.8	38.8
Middle	7.1	0.6	52.7	39.6
Tail	11.1	—	48.9	40

TABLE 5

	Ni (metal)	Periclase-type	Spinel $MgAl_2O_4$
Head	0.35246(5)	0.42054(3)	0.80858(4)
Middle	0.35227(3)	0.42076(2)	0.80836(3)
Tail	0.35210(3)	0.42106(3)	0.80828(4)

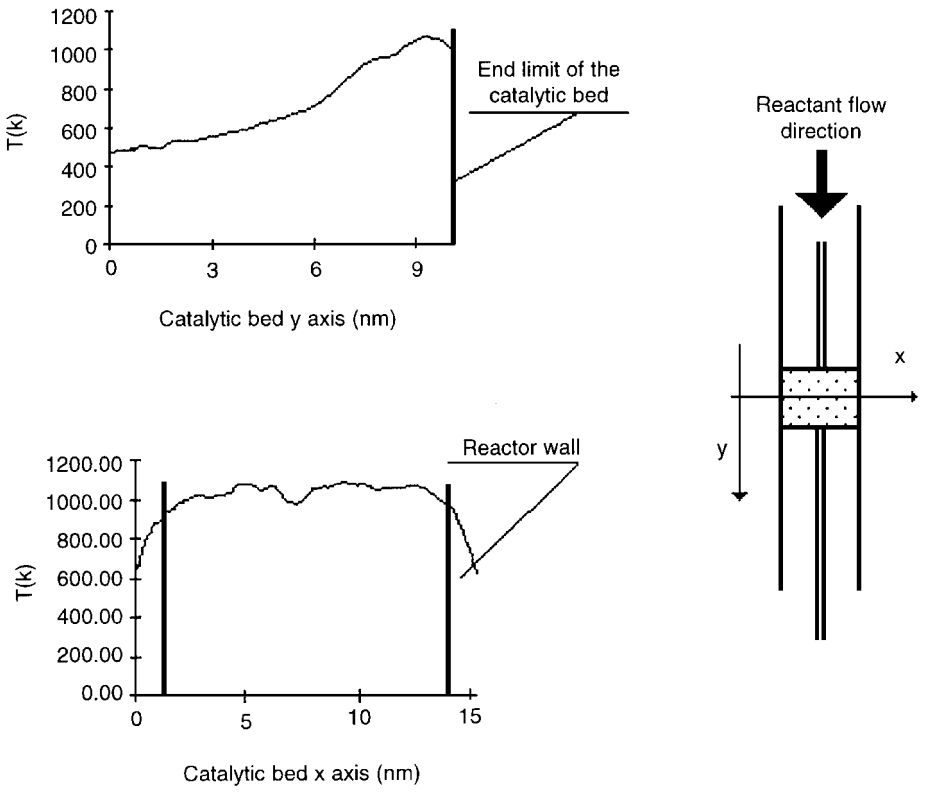

FIG. 3. Radial (A) and longitudinal temperature profiles of the catalytic bed measured with IR thermography during the 14-ms residence time test.

expected weight ratios Ni : MgO : $MgAl_2O_3$ = 13 : 41 : 46 estimated on the basis of chemical analysis. These features can be explained, assuming that part of the Ni atoms were included in very small clusters with diameters lower that 30 Å, while part of the aluminum atoms were included in quasi-amorphous aluminum oxide particles. The latter can explain the weak diffraction halos of Fig. 4. The higher weight percentages of the MgO phase would consequently be related to the incomplete detection of Ni and Al containing phases. The other possible hypothesis which considers that part of the Ni atoms could be included in the MgO peryclase structure was excluded after the analysis the Ni occupancy factors performed according to the Rietveld method.

Concerning the cell parameters, the (a) values for Ni and $MgAl_2O_3$ were very close to the ones of the pure phases, which are 0.35238 and 0.80831 nm, respectively (see also Table 4); whereas the (a) parameter of the periclase-type phases was close to the one of pure MgO only in the tail fraction; being in the head and middle fractions downward shifted by the presence of the NiO contribution (a = 0.41684 nm).

Despite no catalyst deactivation was observed during the 8-h CPO test a constant amount of carbon (10 wt%) was detected in the three fractions of the catalytic bed, both with XRD quantitative phase analysis and with elemental chemical analysis. We have not investigated the carbon formation reactions, however, since no catalyst deactivation was observed along 6 h of reaction and since the same amount of carbon was detected in the three fractions of catalytic bed, we assume that carbon formation occurred in transient conditions during the start up and/or shut down procedures.

The emissivity of the three zones of reaction, 0.61 (head), 0.63 (middle), 0.68 (tail) was estimated through a summation of literature values of the pure identified phases

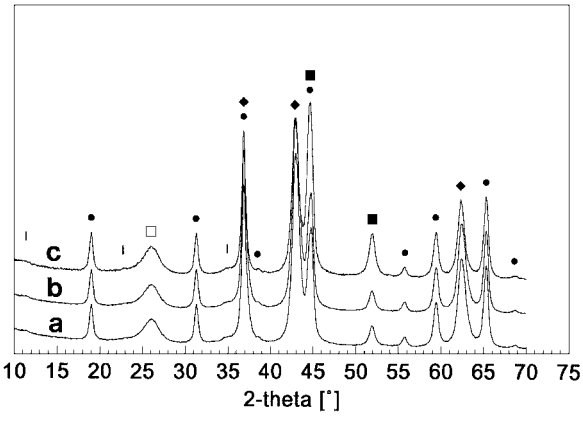

FIG. 4. XRD peaks of the three fractions of the catalytic bed: (a) head, (b) middle, (c) tail. (■) Ni metallic phase, (◆) NiO phase, (□) graphitic phase, (●) $MgAl_2O_4$ spinel phase, (|) diffraction halos attributable to quasi-amorphous Al_2O_3.

(28, 29) multiplied by the weight fractions of the same phases.

4. DISCUSSION

Catalyst Deactivation Phenomena

Previous works performed on samples Ni_{10}, Ni_{34}, Ni_{61}, Ni_{71} showed that calcination at intermediate temperatures (with maximum at about 723 K, corresponding to the disappearance of the HT XRD pattern) gave rise to significant increases in the surface area (typically from 75–80 m^2/g to 170–180 m^2/g) and to unimodal pore distributions, with sharp maxima centered at about 10 nm of pore diameter (12, 13). These results can be related to the desorption of water and CO_2 escaping through the holes in the surface without any extensive change in crystal morphology (30). However, the surface areas dramatically decreased (below 50 m^2/g) at higher calcination temperatures ($\geq$1173 K), due to a structural rearrangement associated with the segregation of spinel and oxide phases (or oxide solid solutions as a function of the relative Ni/Mg/Al ratios). Samples of Ni_{10} and Ni_{34} calcined at $T \geq 1173$ K were strongly hindered toward reduction; this behavior, previously investigated by either XRD analysis or NaOH-leaching tests (12, 13), can be attributed to the segregation of NiO/MgO solid solutions in which the Ni^{2+} species are stabilized inside an inert MgO-type matrix. On the contrary, this stability towards reduction was not observed for the samples Ni_{71} and Ni_{61}, which during the high-temperature calcination step formed NiO crystallites.

It may be assumed that both the high reactivity and the rapid deactivation of the catalysts Ni_{71} and Ni_{61} (64.2 and 57.6 wt% of nickel, respectively) were related to the easy reducibility of the large NiO crystallites, which should originate large Ni-particles that are very reactive towards CPO and towards carbon formation reactions [6]–[7]. Indeed, we observed an extensive formation of carbon on the samples, which occluded the catalytic bed:

$$CH_4 \rightarrow C + 2\,H_2 \qquad [6]$$

$$2\,CO \rightarrow C + CO_2. \qquad [7]$$

A large number of studies have been devoted in the past to the carbon formation reaction and some of them are reported in references (31–35); these studies clearly showed that the reactions [6] and [7] occurred on large Ni-aggregates, while they were kinetically inhibited on small Ni-clusters. Furthermore, it should also be mentioned that, at the end of the catalytic tests, the formation of a thin Ni^0 layer was observed along the reactor walls after the catalytic bed as a result of the formation, followed by decomposition, of volatile $Ni(CO)_4$.

Deactivation was not observed for the Ni_{34} and Ni_{10} catalysts even after 500 h of time-on-stream. In this case the reduction of the (NiO/MgO) solid solution gave rise to well dispersed Ni^0 particles (a fraction of them with dimensions smaller than the ones detectable with XRD analysis), which were stable in the reaction conditions. Similar observations have been previously reported by Gadalla *et al.*, which studied the steam- and/or CO_2-reforming reactions using catalysts obtained by reduction of NiO–MgO solid solutions (36–38).

Reactivity Dependence on Residence Time and Temperature Values

All reactivity tests were performed in laminar flow condition, as normally occurs in laboratory scale experiments utilizing small plug flow reactors and low reactant flow rates. In the shorter residence time range, in the 4 mm ID reactor, particle Reynolds (Re) numbers were lower than 5 (τ was varied between 3.6 and 72 ms by changing both the catalyst amount and the flow rate of reactants) while $Re = 0.2$–10, during the experiments performed in the 15 mm ID reactor (τ was varied between 360 and 10 ms changing the reactant flow rates and leaving unchanged the amount of catalyst, 1500 mg).

Re values do not lead to conclude that changes in reactivity features, observed at residence time values between 720 and 3.6 ms, could be simply attributable to changes in heat or mass transfer coefficients. Nevertheless, the ratios between reaction heat and external heat supply increased by decreasing τ and, at very small residence time, the reactions could be self-sustained. At $\tau < 15$ ms IR thermography and thermocouple measurements also showed that relatively large temperature gradients (between 100–50 K) were originated in the solid–gas interphase region, the surfaces being hotter than gas phase. Conclusively, at very short residence time condition after ignition, surface reactions were efficiently activated by the same heat they produce at the catalytic sites thus avoiding or reducing the need for preheating the reactant gases and reducing heat transfer limitation on reaction rates.

There are also experimental findings indicating that CPO occurred under kinetic control at least at temperatures below 1000 K. In fact experimental data obtained with the 4 mm ID reactor in the residence time range $\tau = 3.6$–72 ms at constant feed composition, showed that: (a) reactions giving rise to high CH_4 conversion and high selectivities towards CO and H_2 were favored at temperatures above 1000 K; (b) reactions which lead to total combustion products were favored below 1000 K; (c) conversion and selectivity values approached the equilibrium ones only above 1000 K.

Differences between experimental and equilibrium compositions observed below 1000 K may be attributed to the high activation energy of some chemical reactions participating in overall equilibria; these reactions with an high activation energy should be those producing CO and H_2, since the selectivity towards these molecules was lower than the

thermodynamic values. Steam-reforming [3] and CO_2-reforming [4] are strongly endothermic reactions with relatively high activation energies and they appear suitable candidates to represent the reactions which are inhibited at temperatures below 1000 K. Therefore, considering only these observations the overall catalytic process, could be described as a two step phenomenon, in which the reforming reactions [3]–[4] follow the total oxidation reactions [2]. However, this formalism does not seem completely adequate to represent all the experimental findings and the points that provoke this inadequacy are underlined as follows.

A first point is made observing that the occurrence of a subsequential two-step mechanism would imply that the secondary reactions, which are inhibited at low-temperature values, namely the reforming ones, should have had reaction rates sufficiently high to explain the observed conversions.

To validate this hypothesis, we ran tests at $\tau = 12$ ms, in the 4 mm ID reactor using feedstocks with a $CH_4/CO_2/He = 1/1/2-0$ v/v and the same Ni_{10} catalyst. These tests were performed at an oven temperature of 1023 K and after a reductive treatment of the catalysts at 1173 K under an H_2/N_2 atmosphere. The temperatures measured in the thermocouple well were close to 1000 K.

Overall turnover frequencies (the number of CH_4 molecules reacted per second per exposed Ni atom, TF_{CH_4}) were then measured in these conditions assuming a 10% Ni dispersion calculated considering the XRD analysis determined a 120 Å average crystal size of Ni ensembles. The obtained results showed that CH_4 conversions were lower than 28% and $TF_{CH_4} = 0.9$–$1.0\ s^{-1}$.

The exam of literature data indicates that CO_2 reforming is slower than steam reforming. In particular, Rostrup-Nielsen and Bak-Hansen (39) measured reaction rates with a catalyst very similar to the Ni_{10} here examined (Ni 16 wt% deposited on a spinel $MgAl_2O_4$ support) and found that TF_{CH_4} was 50% higher during steam reforming than during CO_2 reforming. Here we observe that an analogous increase would move TF_{CH_4} values measured in our experiments in the range between 1.4–$1.5\ s^{-1}$.

In case of the CPO test performed at the $\tau = 12$ ms (T = 1000 K and feedstock $CH_4/O_2/He = 2/1/4$), we obtained an overall $TF_{CH_4} = 4.5\ s^{-1}$ and a CH_4 conversion = 92%. However, the number of CH_4 molecules reacted per second in steam and CO_2 reforming reactions [3]–[4] results higher. This was estimated on the basis of two assumptions: (a) reaction mechanisms consist of an initial total oxidation [2] which goes to completion and is followed by steam and CO_2 reforming according to Eqs. [3]–[4]; (b) only Ni atoms in a reduced form (30% of total according to Table 4 results) are able to catalyze steam and CO_2 reforming reactions.

Following these assumptions we estimated that $TF_{CH_4} = 10\ s^{-1}$; a number which significantly higher than the corresponding one (between 1–$1.5\ s^{-1}$) estimated for the reactions occurring in the absence of oxygen.

This increase of TF_{CH_4} in a two step CPO could be partly justified by observing that during short residence time CPO, the CO_2 and the H_2O molecules (as well as the heat for activating the reactions) were generated at the surface. However, CH_4 molecules were still supplied to the catalytic sites from the gaseous phase with mass transfer rates characteristic of laminar flow conditions, limiting the overall velocity of the catalytic process.

A second and stronger point is suggested by the surface and gas temperature profiles measurements and by the chemical and phase analysis of the three sections of the catalytic bed. Literature data (7) indicate that when CPO is performed at high residence time conditions ($\tau \cong 300$ ms) the highest temperatures are produced in the first section of the catalytic bed while the lowest temperatures are characteristic of subsequent zones. Indeed, our observation performed at $\tau > 70$ ms were consistent with the literature information.

Instead, the experiments at $\tau < 70$ ms and in particular the experiment at $\tau = 14$ ms in the 15 mm ID reactor, showed completely different features. In fact IR thermography and thermocouple measurements showed that both surface and gas temperatures were the highest in the very last part of the catalytic bed which was incandescent (see also Figs. 2 and 3), whereas the initial and middle sections of the catalytic bed were at much lower temperatures. These experimental indications are not consistent with a two step mechanism description since in case of total oxidation followed by steam and CO_2 reforming reactions and water gas shift, it would be expected that a "hot zone," where exothermic total oxidation occurs, should be placed before a "cool zone" where endothermic steam and CO_2 reforming take place. In addition as, already mentioned, the hot "tail" zone contained only Ni in a metallic phase; while Ni would have been expected in an oxidized NiO phase if this zone had had catalyzed total oxidation (40).

Independently from the formalism used to represent reaction mechanisms, what is more relevant in the presented data is the observation that the temperature gradients and phase composition differences, point out that there is a discontinuity between the chemical phenomena which originate CPO in the wide range of residence time here examined.

Further work is in progress to investigate, with spectroscopic means, the relationships between surface molecular properties, temperature, and residence time conditions.

ACKNOWLEDGMENTS

Thanks are due to Dr. M. Gazzano (CSFM-CNR, Bologna, Italy) for XRD characterization and Dr. M. A. Pena (Inst. de Catalysis y Petroleoquimica-CSIC, Madrid, Spain) for useful suggestions. Special thanks

are due to P. Visioli (Snamprogetti SpA, San Donato Milanese, Italy) for his patient and skilled technical assistance.

REFERENCES

1. Hickman, D. A., and Schmidt, L. D., *J. Catal.* **138**, 267 (1992).
2. Huff, M., and Schmidt, L. D., *J. Phys. Chem.* **97**, 11815 (1993).
3. Hickman, D. A., and Schmidt, L. D., *Science* **259**, 343 (1993).
4. Choudhary, V. R., Mamman, A. S., and Sansare, S. D., *Angew. Chem. Int. Ed. Engl.* **31**, 1189 (1992).
5. Choudhary, V. R., Rajput, A. M., and Rane, V. H., *J. Phys. Chem.* **96**, 8686 (1992).
6. Choudhary, V. R., Rajput, A. M., and Prabhakar, B., *J. Catal.* **139**, 326 (1993).
7. Dissanayake, D., Rosinek, M. P., Kharas, K. C. C., and Lunsford, J. H., *J. Catal.* **132**, 117 (1991).
8. Prettre, M., Eichner, Ch., and Perrin, M., *Trans. Faraday Soc.* **43**, 355 (1946).
9. Basini, L., Aragno, A., and Vlaic, G., *Catal. Lett.* **39**, 49 (1996).
10. Chang, Y.-F., and Heinemann, H., *Catal. Lett.* **21**, 215 (1993).
11. Dissanayake, D., Rosynek, M. P., and Lunsford, J. H., *J. Phys. Chem.* **97**, 3644 (1993).
12. Clause, O., Goncalves Coelho, M., Gazzano, M., Matteuzzi, D., Trifirò, F., and Vaccari, A., *Appl. Clay Sci.* **8**, 169 (1993).
13. Fornasari, G., Gazzano, M., Matteuzzi, D., Trifirò, F., and Vaccari, A., *Appl. Clay Sci.* **10**, 69 (1995).
14. Young, R. A., "The Rietveld Method," International Union of Cristallography, University Press, Oxford, 1993.
15. Hill, R. J., and Howard, C. J., *Appl. Cryst.* **20**, 467 (1987).
16. Schneider, J., WRIET version 3, powder profile refinement and structure analysis package for personal computers, University of Munich (BRD).
17. Wyckoff, R. W. G., *Crystal Structures*, Interscience, New York, 1963.
18. Clause, O., Gazzano, M., Trifirò, F., Vaccari, A., and Zatorski, L., *Appl. Catal.* **73**, 217 (1991).
19. Cavani, F., Trifirò, F., and Vaccari, A., *Catal. Today* **11**, 173 (1991).
20. Trifirò, F., and Vaccari, A., *in* "Comprehensive Supramolecular Chemistry" (J. L. Atwood, J. E. D. Davies, D. D. MacNicol, and F. Vögtle, Eds.), Vol. 7, Chap. 8, Pergamon, Oxford, 1996.
21. West, A. R., "Solid State Chemistry and its Application," Chap. 10, Wiley, Chichester, 1984.
22. "Powder Diffraction File of Inorganic Phases," International Centre for Diffraction Data, Swarthmore, PA, 1991.
23. Delmon, B., "Introduction a la Cinétique Hétérogène," Technip, Paris, 1969.
24. Boldirev, V. V., Bulens, M., and Delmon, B., "The Control of the Reactivity of Solids," Elsevier, Amsterdam, 1979.
25. Trifirò, F., Vaccari, A., Clause, O., and Gazzano, M., *in* "Proc. 2nd Europ. Conference on Advanced Materials and Processes" (T. W. Clyne and P. J. Withers, Eds.), Vol. 3, p. 304, Institute of Materials, London, 1992.
26. Bond, C. G., and Sarsam, S. P., *Appl. Catal.* **38**, 365 (1988).
27. Vaccari, A., and Gazzano, M., *in* "Preparation of Catalysts VI" (G. Poncelet, J. Martens, B. Delmon, P. A. Jacobs, and P. Grange, Eds.), p. 893, Elsevier, Amsterdam, 1995.
28. G. V., Samsonov (Ed.), "The Oxide Handbook," IFI/Plenum, New York, 1982.
29. White, F. M., "Heat Transfer," Addison–Wesley, Reading, MA, 1984.
30. Reichle, W. T., Kang, S. Y., and Everhardt, D. S., *J. Catal.* **101**, 352 (1986).
31. Rostrup-Nielsen, J. R., "Steam Reforming Catalysts," Teknisk Forlag, Copenhagen, 1975.
32. Bernardo, C. A., Alstrup, I., and Rostrup-Nielsen, J. R., *J. Catal.* **96**, 517 (1985).
33. de Bokx, P. K., Kock, A. J. M., Boellaard, E., Klop, W., and Geus, J. W., *J. Catal.* **96**, 454 (1985).
34. Manning, M. P., Garmirian, J. E., and Reid, R. C., *I.&E.C., Process Des. Dev.* **21**, 404 (1982).
35. Rostrup-Nielsen, J. R., *J. Catal.* **85**, 31 (1984).
36. Gadalla, A. M., and Sommer, H. E., *J. Am. Cer. Soc.* **72**, 683 (1989).
37. Gadalla, A. M., and Bower, B., *Chem. Eng. Sci.* **43**, 3049 (1988).
38. Gadalla, A. M., and Sommer, M. E., *Chem. Eng. Sci.* **44**, 2825 (1989).
39. Rostrup-Nielsen, J. R., and Bak Hansen, J.-H., *J. Catal.* **144**, 38 (1993).
40. Mc Carty, J. G., *Catal. Today* **26**, 283 (1995).